Pre-print version of the article published in:
Appl. Surf. Sci. 290 (2014); 27 - 34
DOI: 10.1016/j.apsusc.2013.10.180

Surface investigations of ZnBeMnSe mixed crystals by means of the piezoelectric spectroscopy and the AFM technique

K. Strzałkowski[1], S. Kulesza[2], J.Zakrzewski[1], M. Maliński[3]

[1]Institute of Physics, Faculty of Physics, Astronomy and Informatics, Nicolaus Copernicus University, Grudziadzka 5, 87-100 Torun, Poland
[2]Department of Mathematics, University of Warmia, ul. Sniadeckich 2, 75–328 Olsztyn, Poland
[3]Department of Electronics, Technical University of Koszalin, ul. Sniadeckich 2, 75–328 Koszalin, Poland
Corresponding author: K. Strzałkowski, skaroll@fizyka.umk.pl, phone: 0048692631318

Abstract

Piezoelectric photoacoustic spectroscopy with a piezoelectric detection has been used for measurements of the amplitude and phase spectra of $Zn_{1-x-y}Be_xMn_ySe$ mixed semiconductors. The investigated crystals were grown from the melt by the modified high pressure Bridgman method under the argon overpressure. The preliminary study of the sample's surface of the investigated crystals was carried out using the AFM technique. The influence of a different surface treatment on the amplitude and phase piezoelectric spectra as well as on AFM images is presented and analyzed. The correlations between these two techniques have been found and are discussed. Piezoelectric (PZE) spectra were analyzed using an extended and modified Jackson-Amer theory.

Keywords: A2B6 semiconductors; AFM technique; Diluted magnetic semiconductors; Mixed crystals; Piezoelectric detection; Surface of semiconductors

1 Introduction

Diluted Magnetic Semiconductors (DMS) are materials with magnetic ions implemented into the crystal structure. These materials are of very high interest because of a potential application in spintronics [1,2] and also optoelectronics. DMS based on II-VI crystals such as ZnBeMnSe mixed compounds with the manganese are very promising materials for spintronics due to their unique magnetic and optical properties [3]. The novel and peculiar magnetic and magnetooptical properties of Mn containing II-VI solid solutions arise from the interaction between charge carriers and the magnetic Mn^{2+} ions placed in the cation site [4]. ZnBeMnSe semiconductors are an interesting material for spintronics as a spin filter layer with possible applications in a memory technology. Schmidt and Molenkamp demonstrated injection of a strongly up to 90% spin-polarized current into a light emitting diode [5]. The leading problem in spintronics is manipulating of the polarization of the carriers in a convenient way without an external magnetic field. Potential solution of this problem could be magnetic resonant tunneling diodes (MRTD) for a voltage control of the spin [6]. MRTD diodes base on III-V compounds but also II-VI semiconductors such as ZnSe, ZnBeSe and ZnMnSe were proposed [7]. There are some crucial advantages of II-VI in comparison with III-V magnetic semiconductors. In II-VI crystals, manganese is an isoelectronic atom, so n-type and p-type doping is possible. Mn^{2+} ions exhibit a relatively high solubility with many II-VI binary compounds. The content of the manganese for a thin layer of $Zn_{1-x}Mn_xSe$ material can be even equal to x=1 [3]. Changing the concentration of the beryllium in $Zn_{1-x-y}Be_xMn_ySe$ crystals allows for lattice-matched growth on GaAs and for alignment of the offset of the conduction band (bandgap and lattice constant engineering [8]). The beryllium in II-VI ternary and quaternary compounds plays also a significant role because of hardening and stabilizing the crystal structure [9,10]. From the application point of view surface investigations of such a material are of high importance. In this work piezoelectric photoacoustic method developed by Jackson and Amer [11] and modified by Maliński [12] was applied as a simple and fast technique for the surface investigation. Up to date several papers have been published concerning interpretation of piezoelectric amplitude and phase spectra of $Zn_{1-x-y}Be_xMn_ySe$ mixed crystals [13-18]. The piezoelectric method turned out to be sensitive on a different sample's surface preparation. In the PZE spectra of these compounds absorption bands appear in the sub-bandgap region whose intensities depend on technological processes of the surface treatment. Since similar effects were observed also for ZnBeMgSe [19] and for binary crystals [20-22], this absorption cannot be explained only on the base of doping or the presence of manganese in ZnBeMnSe semiconductors. It was assumed that these bands are connected with the state of the surface of the investigated crystals. Since the physical nature of these absorption bands remains still uncertain other measurement techniques are welcome to confirm results obtained with the piezoelectric photoacoustic spectroscopy. In this paper as a new method to characterize the surface of the investigated samples AFM technique was applied. The aim of this article is to present and discuss the influence of the sample surface preparation process on the piezoelectric photoacoustic amplitude and phase spectra of mixed $Zn_{1-x-y}Be_xMn_ySe$ compounds and check if the correlations with the AFM technique can be found.

2 Material and methods

The crystals were grown from high purity powders of ZnSe, Be, Mn and Se with the high pressure modified Bridgman method under argon overpressure of about 150 atm. The crystal rods were etched in HCl and next cut into about 1.5 mm thick plates. The samples were first ground using grinding powder (Al_2O_3, 10 μm in diameter), next polished with diamond paste (1 μm) and finally chemically etched in a solution of sulfuric acid (96%), potassium dichromate and water. After etching, the samples were rinsed in distilled water and then put for a few seconds into boiling sodium hydroxide. Then the samples were rinsed again in cold and next in boiling distilled water and finally in ethyl alcohol. Some samples after polishing were annealed in zinc vapour at 1300 K for 48 hours. After each step of the surface treatment photoacoustic amplitude and phase spectra were measured as well as AFM images were taken.

A typical experimental setup for the piezoelectric photoacoustic spectroscopy with a computer-controlled measurement was applied. Samples were illuminated with the intensity-modulated beam of light of a xenon lamp (Cermax 300 W) after passing through the prism monochromator. A PZE cell with the piezoelectric detection has been used with a construction allowing performing measurements in two experimental configurations (modes). When the incident light impinges the sample from the same side as the detector one calls it a front mode otherwise a mode is called rear [15]. The piezoelectric signal was detected with a lock-in phase selective amplifier (Stanford SR 510) at room temperature in both experimental configurations. The AFM measurements were carried out using Multimode 8 Atomic Force Microscope (Bruker) in a MFM (Magnetic Force Microscopy) mode. MFM uses a combination of a tapping mode and a lift mode of the microscope together with a magnetic probe to gather information about the magnetic field above the sample. Each line of the sample is first scanned at a low tip-surface distance to obtain the sample topography and then the probe is lifted to a given height, and the line is retraced to collect the magnetic data. A lateral resolution of the sample topography is limited by the tip radius (20 nm for MESP). On the other hand, the MFM resolution is roughly equal to the lift height (not better than 20-50 nm), although additional van der Waals forces might influence the tip-surface interactions at very low lift values. The MESP probe characteristics: tip radius 20 nm, resonant frequency 75 kHz, spring constant 2.8 N/m, magnetic coating (10-150 nm of Co/Cr), coercivity 400 Oe.

3 Theory

Computations of the piezoelectric spectra were performed for an optical absorption coefficient $\beta(E)$ spectrum for the photon energies below and above the energy gap (E_g) of the crystal, represented by the formulae (1) and (2) respectively:

$$\beta(E) = \beta_0 \cdot \exp\left(\frac{(E - E_g)\cdot\gamma}{0.025}\right) \quad \text{for} \quad E<E_g \quad (1)$$

$$\beta(E) = A_0(E - E_g)^{1/2} \quad \text{for} \quad E>E_g \quad (2)$$

where β_o, γ, A_o are the parameters. Equation 1 describes the Urbach tail thermal broadening of the absorption band observed for all direct electron type transition semiconductors. The second formula describes the absorption band connected with the direct, band-to-band, electron transitions in semiconductors. Considering a non-perfect crystal, one must assume the presence of a very thin surface layer of a thickness *d* with a thermal conductivity and an absorption coefficient spectrum different from the volume of the sample. The surface type optical absorption coefficient spectrum connected with the presence of the defected layer can be given in the form of the Gaussian distribution (Eq. 3):

$$\beta(E) = A_{1/2} \cdot \exp\left(\frac{E - E_{1/2}}{\beta_{1/2}}\right)^2 \qquad (3)$$

where $A_{1/2}$ and $\beta_{1/2}$ are parameters, $E_{1/2}$ are energy locations of defects.

The piezoelectric signal *S* can be then expressed by the following formula [12]:

$$S \cong \frac{1}{l}\int_0^l T(x,\beta)dx \pm \frac{6}{l^2}\int_0^l \left(\frac{l}{2} - x\right)T(x,\beta)dx \qquad (4)$$

where $T(x,\beta)$ is the total temperature distribution field in the sample associated with the surface defects and volume absorption, *x* is the spatial coordinate and *l* is the thickness of the sample. The first part of Eq. 4 describes a thermal expansion of the whole volume of the sample (piston effect) and the second one bending of it (drum effect). The piston effect dominates when the absorption of the light takes place in the whole volume of the sample (low absorption region, below the energy gap). The role of a drum effect increases when the light is absorbed only in a thin layer of the sample (high absorption region, above the energy gap). In the front mode these two effects add up and in the rear one the subtraction takes place [14-22]. The total piezoelectric signal is always a combination of these two components. Theoretical predictions for the amplitude and phase spectra for the perfect crystal without an absorption below the energy gap in the rear (a) and front (b) measurement configurations respectively are presented in Fig. 1. A characteristic peak in the sub-bandgap region in the amplitude spectrum for the rear case is visible. According to the Jackson-Amer theory, the peak is due to subtracting the components coming from the piston and drum effect in the rear configuration mode. For the same reason the phase spectrum goes down and changes sign, in contrast to the front mode, where only slight change of the phase is observed. For the real samples the quality of the crystal, the samples preparation method and the measurement setup are very important; hence the proper interpretation of the real PZE spectra can be often difficult. However, the goal is to prepare the samples for the measurement in such a way, that the measured spectra will come closer to the perfect ones.

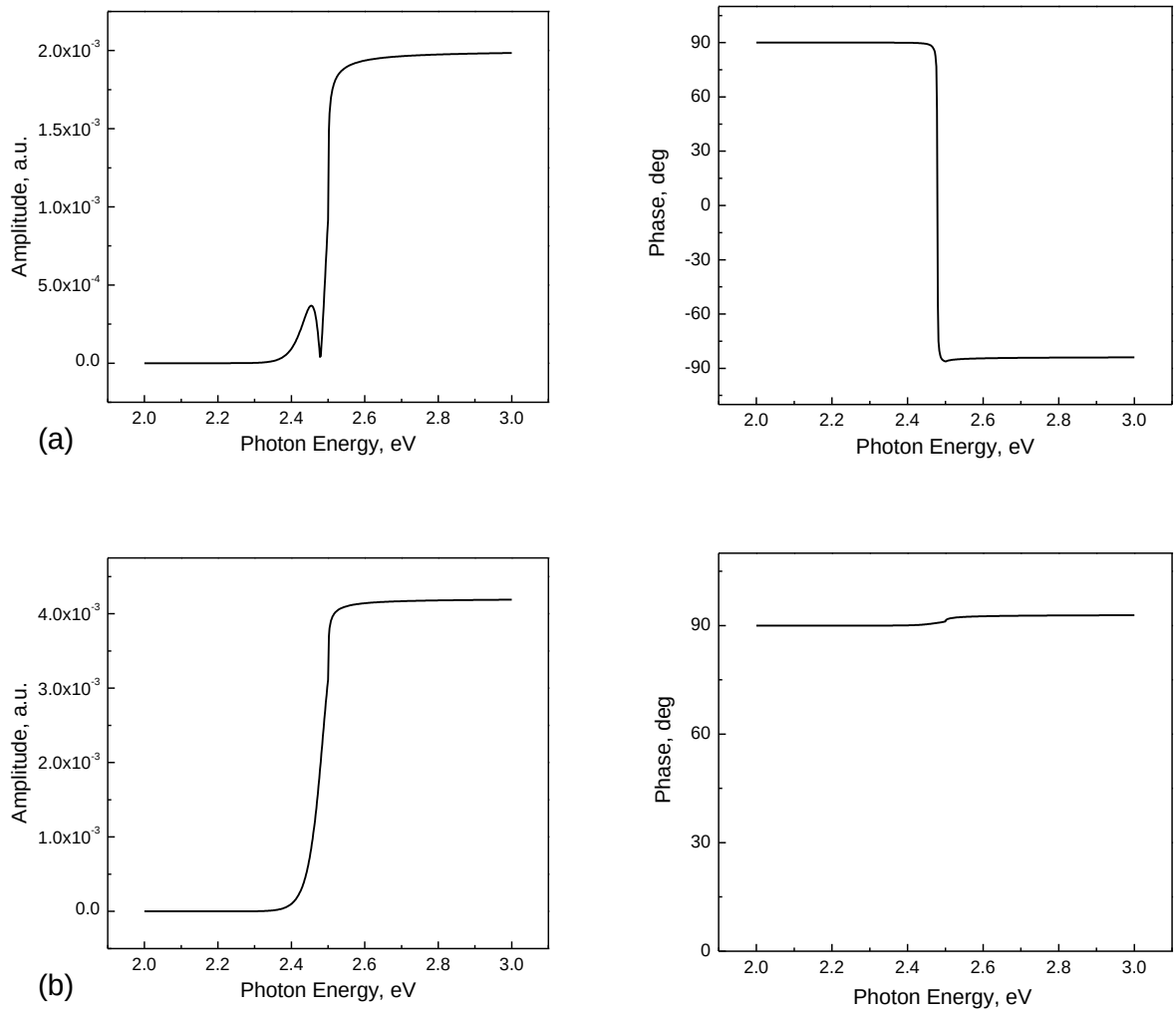

Fig. 1 Theoretical predictions for the amplitude and phase spectra in the rear (a) and the front (b) mode respectively for a set of parameters: $\alpha = 5 \cdot 10^{-6}$ m$^2 \cdot$s^{-1}, l=0.1 cm, f=36 Hz, E_g=2.5 eV, γ=1.

4 Results and discussion

Figure 2 presents the experimental amplitude and phase PZE spectra measured at the modulation frequency 36 Hz for different preparation of the surface for $Zn_{0.85}Be_{0.1}Mn_{0.05}Se$ sample in the front mode (a) and for $Zn_{0.9}Be_{0.05}Mn_{0.05}Se$ crystal in the rear mode (b). In contrast to ground and polished samples for the etched ones the strong increase of the ratio of the amplitude signal at high absorption to that at low absorption region is clearly seen. This effect is due to the stronger scattering of the incident light in the case of ground and polished crystals comparing the etched one. For the ground sample in both, front and rear cases, intense peaks in the amplitude at energies about 2.85 eV (a) and 2.73 eV (b) can be observed, whose intensity depends on the surface treatment. Appropriate changes in the phase are also clearly visible. Since the intensity of the peak decreases after polishing and etching and at the same time the increase of the amplitude in the high absorption region is observed, it must be connected with the surface of the crystal [15].

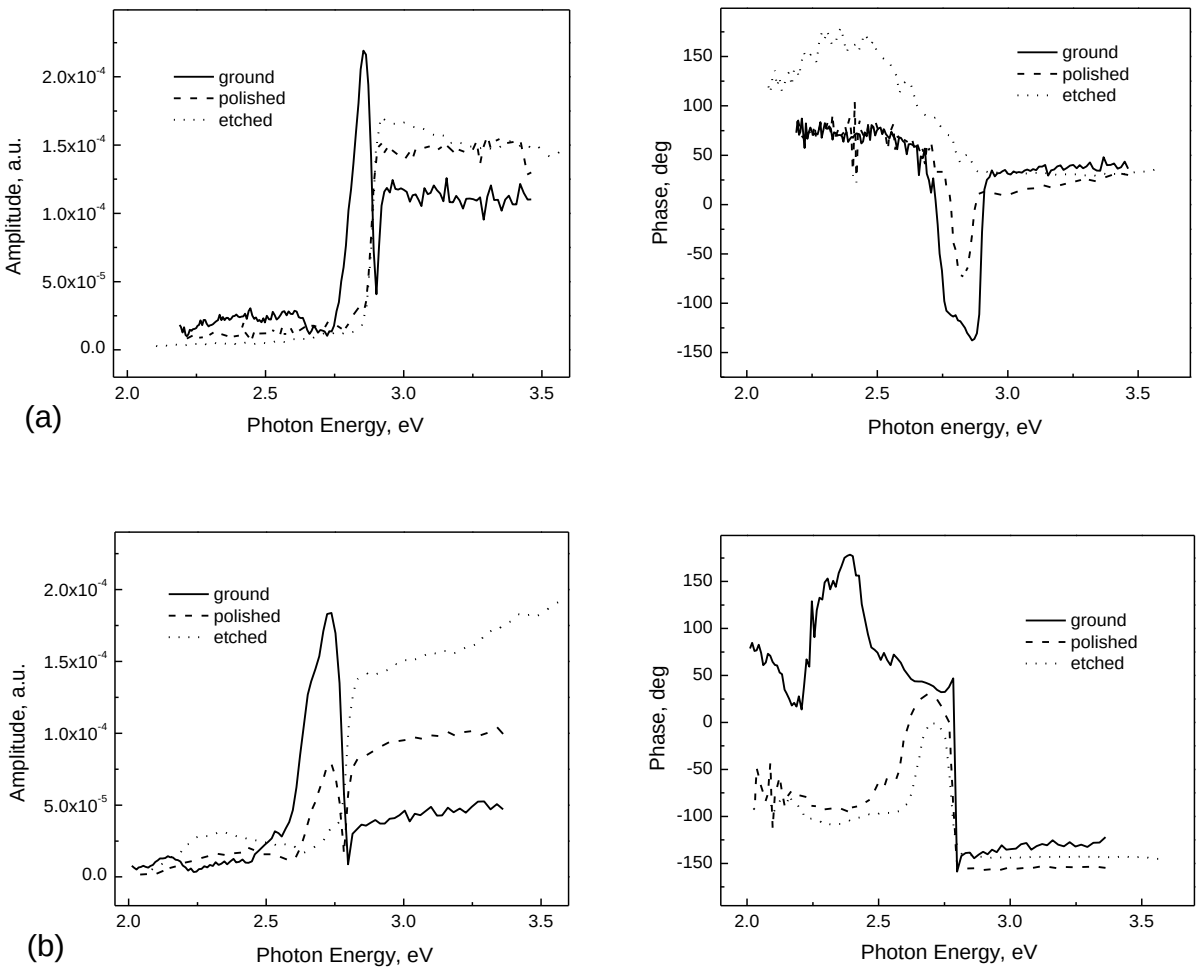

Fig. 2 PZE amplitude and phase spectra measured at f=36 Hz for different preparation of the surface for $Zn_{0.85}Be_{0.1}Mn_{0.05}Se$ and $Zn_{0.9}Be_{0.05}Mn_{0.05}Se$ crystals in the front (a) and in the rear mode (b) respectively.

Amplitude and phase spectra measured in the rear mode for $Zn_{0.9}Be_{0.05}Mn_{0.05}Se$ polished (a) and etched (b) samples measured at the following chopping frequencies: 6 Hz (line), 76 Hz (dash) and 226 Hz (dot) are presented in Fig. 3. A maximum of the amplitude signal was observed at the energy 2.76 eV for both polished and etched samples at high frequencies of modulation. The higher modulation frequency f means the smaller thermal diffusion length and the PZE signal is generated at the smaller depth. Thermal diffusion length μ is given by the expression: $\mu = (\alpha/\pi f)^{1/2}$. The thermal diffusivity α of a typical mixed II-VI crystal is of the order of $2 \cdot 10^{-6}$ m^2/s [23,24]. Thermal diffusion lengths calculated for 6, 76 and 226 Hz are 300, 90 and 50 μm respectively. These values are much smaller than the average thickness of the investigated samples (1.5 mm). Hence the increase of the intensity of the peak is observed and simultaneously the influence of the signal sources coming from the surface on the total signal is increasing. Thus the nature of this peak must be associated with the surface of the sample.

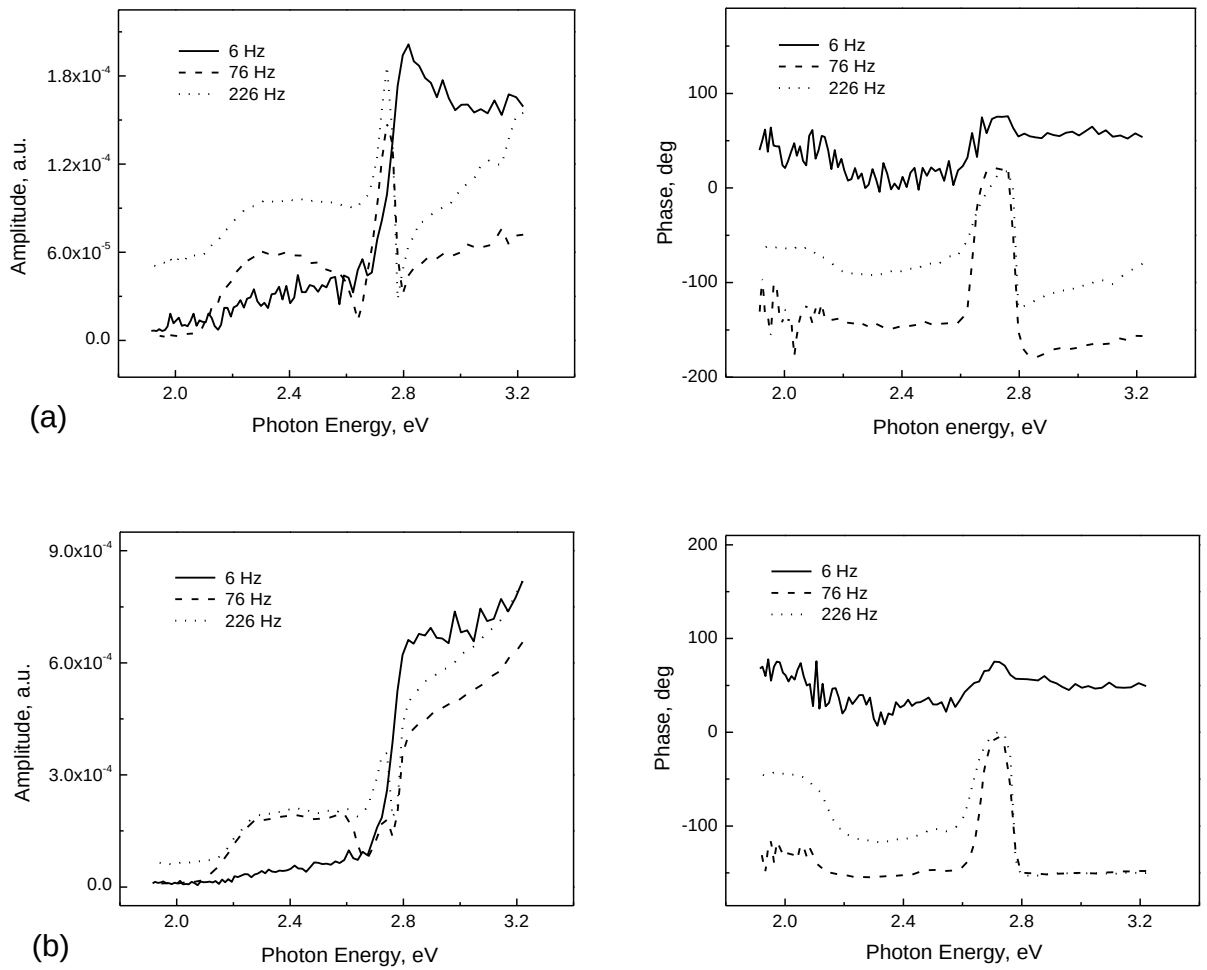

Fig. 3 Amplitude and phase spectra collected in the rear mode for $Zn_{0.9}Be_{0.05}Mn_{0.05}Se$ polished (a) and etched (b) sample at following frequencies: 6 Hz (line), 76 Hz (dash) and 226 Hz (dot).

As an example of theoretical calculations in the case of the non-perfect crystal, experimental (circle) as well as theoretical (line) results for $Zn_{0.85}Be_{0.05}Mn_{0.1}Se$ crystal in the rear mode for the amplitude (a) and the phase (b) were presented in Fig. 4. In the amplitude spectrum absorption bands in the sub-bandgap region connected with surface absorption can be seen. In the phase spectrum they are manifested as a drop of the phase. Two absorption bands positioned at energies 2.35 eV and 2.6 eV respectively have been assumed. Thickness *d* of the defected layer obtained from the fitting procedure was as about 10 μm. It was shown numerically that in the case of pure II-VI semiconductors thickness *d* can vary from 10 μm up to 100 μm [22]. These values remain in a good agreement with the results of thermal diffusion lengths obtained for different chopping frequencies.

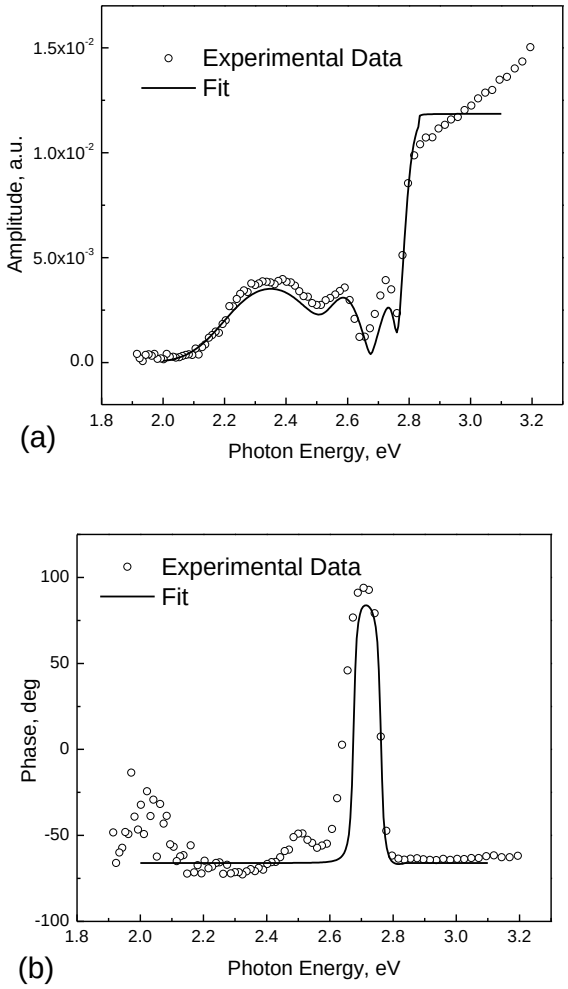

Fig. 4 Experimental (circle) and theoretical (line) spectra in the rear mode for the amplitude (a) and phase (b) for the $Zn_{0.85}Be_{0.05}Mn_{0.1}Se$ crystal. The following set of parameters was used for calculations: $\alpha = 3 \cdot 10^{-6}$ m$^2 \cdot$s^{-1}, l=0.1 cm, f=76 Hz, E_g=2.82 eV, γ=0.8, A_1=360 cm^{-1}, E_1=2.35 eV, A_2=300 cm^{-1}, E_2=2.6 eV.

In Fig. 5 amplitude spectra measured for $Zn_{0.9}Be_{0.05}Mn_{0.05}Se$ annealed sample in the rear mode at different modulation frequencies are given. In measured spectra there are no absorption bands below the energy gap for all applied frequencies. It is known that the annealing process improves the quality of the crystal because of the reduction of zinc vacancies. The annealing process seems also to stabilize the surface of the crystal.
Figures 6, 7, 8 and 9 present AFM images of $Zn_{0.9}Be_{0.05}Mn_{0.05}Se$ crystals ground, polished, etched and annealed respectively. The topography of the surface of the ground sample is very rough (RMS = 215 nm over 5×5 μm^2 scan area), exhibiting neither a pronounced lay nor any regular surface structure. The irregular sample topography resembles a sandblasted or chemically etched surface. A polished sample exhibits a highly inhomogeneous topography: surface roughness (RMS value) equals to 21 nm when measured over 10×10 μm^2 scan area, but at the same time a number of cavities with the depth of 300 nm and diameter of about 500 nm can be seen on the surface, which is atomically flat otherwise (long scratches with the depth of 0.5 nm).

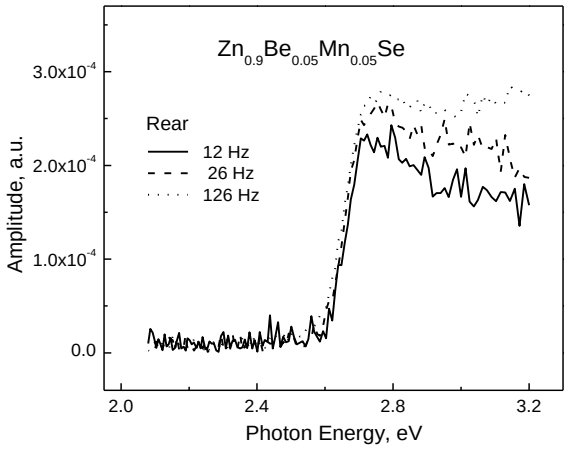

Fig. 5 PZE amplitude spectra collected at different frequencies for different surface treatment for the $Zn_{0.9}Be_{0.05}Mn_{0.05}Se$ annealed crystal in the rear mode.

The roughness of the surface of the etched sample is less than 10 nm (5×5 μm^2); it exhibits regular and parallel scratches (5-10 nm deep, 20-50 nm wide). Apart from that, numerous seeds of a foreign material with the diameter smaller than 20 nm are seen (probably residual particles from technological processes). The seed concentration was estimated to be 3×10^{10} cm^{-2}. The annealed sample is very flat (surface roughness smaller than 5 nm) with tiny, parallel scratches up to 1 nm in depth together with seed particles with the diameter of 200 nm, the height approaching 100 nm, and the concentration 1.5×10^{9} cm^{-2}. The ground sample exhibits the greatest roughness; on the other hand the annealed sample the smallest. Every step of the surface treatment improves the quality of the surface, which is in agreement with results obtained from the piezoelectric photoacoustic spectroscopy. However, obtained results are not consistent quantitatively. The thickness of the defected layer derived from numerical calculations is two orders of magnitude greater than the average roughness of the surface of the investigated samples. To verify quantitatively obtained results it is important to measure the thickness of the defected layer with another experimental technique like Augers Electron Spectroscopy or Positron Annihilation Spectroscopy.

5 Conclusions

The experimental amplitude piezoelectric photoacoustic spectra presented in this paper for the different surface treatment and different frequencies of modulation confirm the assumption about surface type absorption in the sub-bandgap region. Due to strong scattering of the light, the piezoelectric spectra in the saturation region for both ground and polished samples, exhibit a deficiency of the piezoelectric amplitude signal for photon energies above the energy gap. Etching of the surface restored in each investigated case the expected high value of the amplitude of the piezoelectric signal. Additional surface stabilizing effects were observed for sample annealed in zinc vapour. From the observations of measured spectra after each step of surface preparation one can state that they are approaching the perfect ones presented in Fig. 1. The same conclusion arises from analyzing of the AFM data. The average roughness of the surface of the investigated samples decreases after each step of the technological process. The increase of the surface quality caused by the surface treatment processes decreased, as it is

believed, the thickness of a defected layer responsible for a deficiency of the piezoelectric signal. The results of this research lead to the final conclusion that the piezoelectric method can be applied successfully for the testing procedure in examination of the quality of surfaces of semiconductor samples after the surface preparation processes. However, to verify obtained results another type of the measurement techniques would be applied in the future.

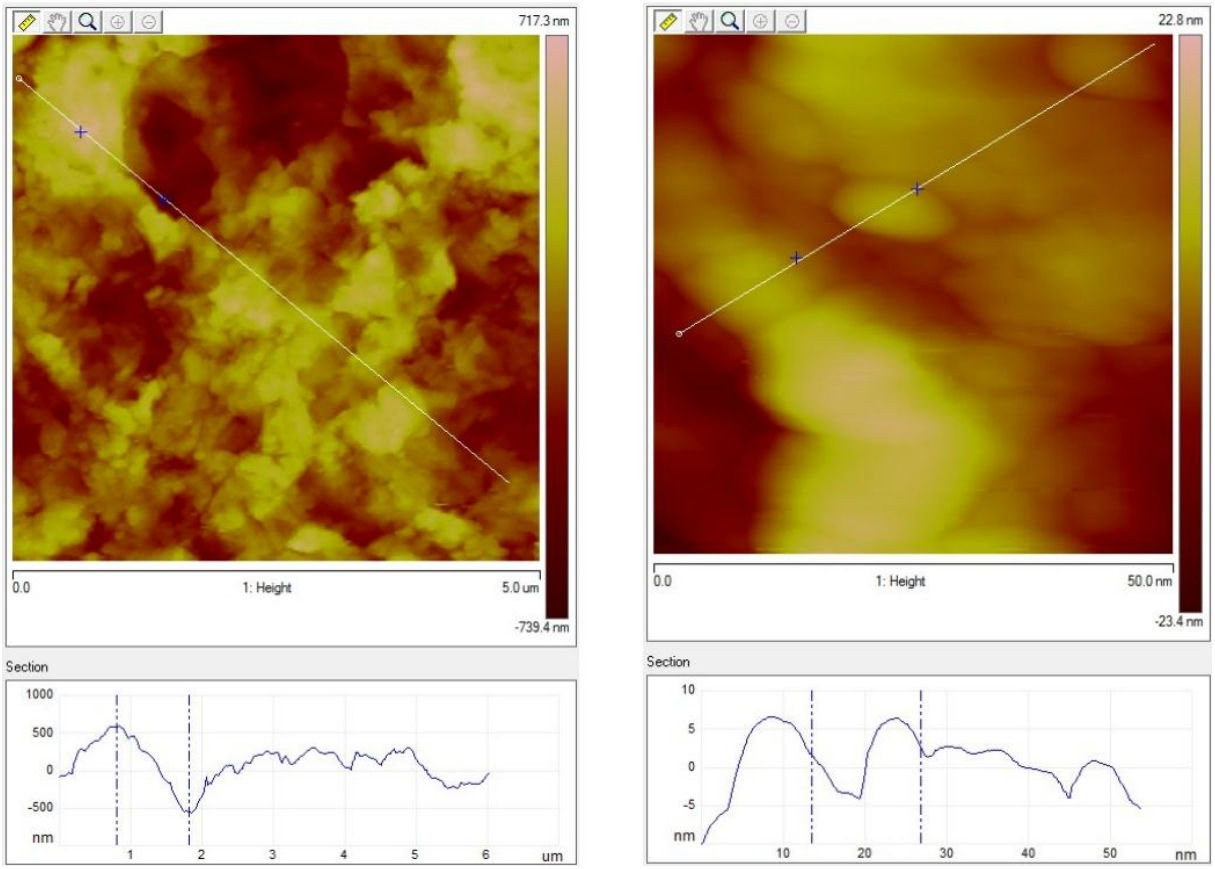

Fig. 6 AFM images of the $Zn_{0.9}Be_{0.05}Mn_{0.05}Se$ ground sample.

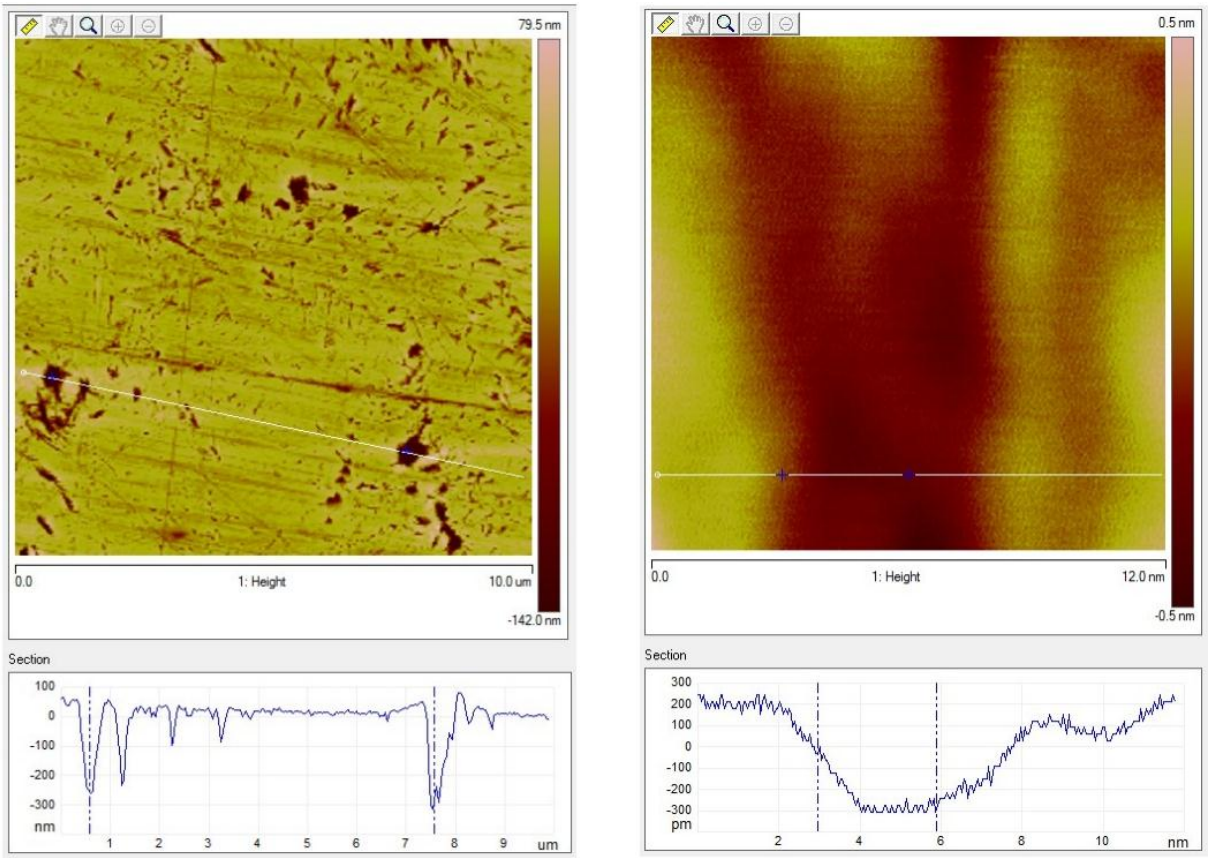

Fig. 7 AFM images of the $Zn_{0.9}Be_{0.05}Mn_{0.05}Se$ polished sample.

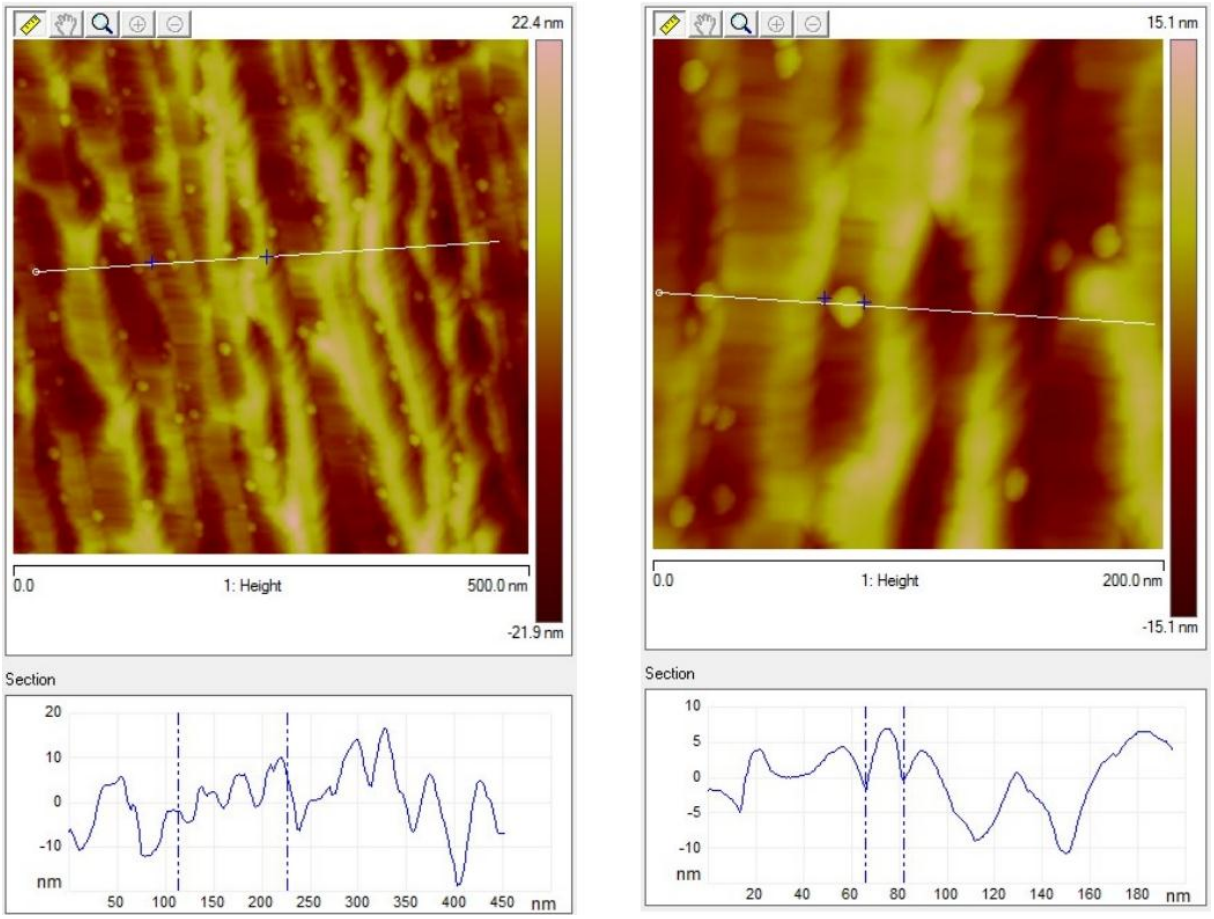

Fig. 8 AFM images of the $Zn_{0.9}Be_{0.05}Mn_{0.05}Se$ etched sample.

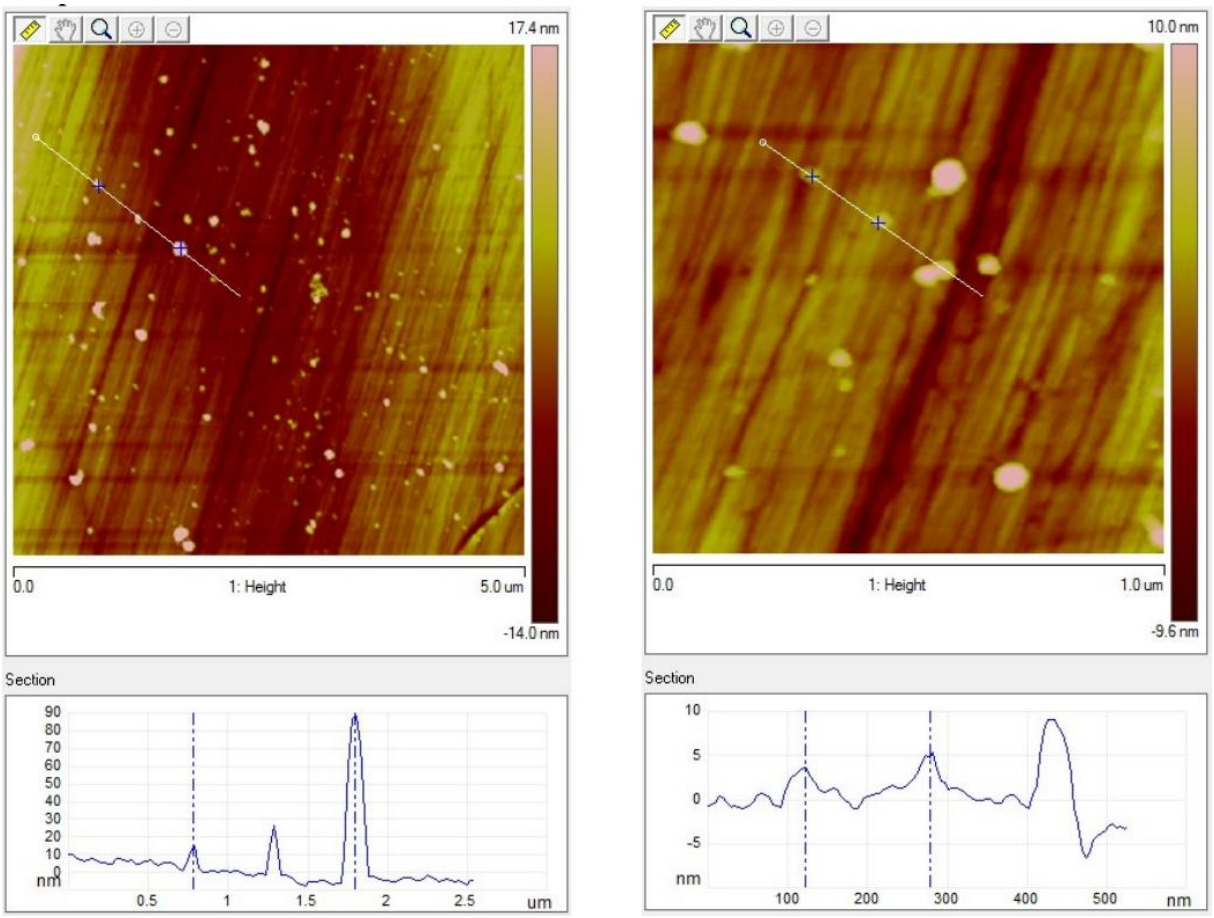

Fig. 9 AFM images of the $Zn_{0.9}Be_{0.05}Mn_{0.05}Se$ annealed sample.

References

[1] R. Fitzgerald, Phys. Today 53 (2000) 21.

[2] S.J. Pearton, C.R. Abernathy, D.P. Norton, A.F. Hebard, Y.D. Park, L.A. Boatner, J.D. Budai, Mat. Sc. and Engineering R 40 (2003) 137.

[3] G. Theurich and N. A. Hill, Phys. Rev. B 66 (2002) 115208.

[4] E. Oh, R. G. Alonso, I. Miotkowski, A. K. Ramdas, Phys. Rev. B 45 (1992) 10934.

[5] G. Schmidt and L.W. Molenkamp, J. Appl. Phys. 89 (2001) 7443.

[6] Christian Ertler and Jaroslav Fabian, Phys. Rev. B 75 (2007) 195323.

[7] A. Slobodskyy, C. Gould, T. Slobodskyy, C. R. Becker, G. Schmidt and L.W. Molenkamp, Phys. Rev. Lett. 90 (2003) 246601-1.

[8] F. Rozpłoch, J. Patyk, F. Firszt, S. Łęgowski, H. Męczynska, J. Zakrzewski, A. Marasek, Phys. Stat. Sol. (b) 229 (2002) 707.

[9] A. Waag, F. Fisher, K. Schül, T. Baron, H.J. Lugauer, Th. Litz, U. Zehnder, W. Ossau, T. Gerhard, M. Keim,G. Reuscher and G. Landwehr, Appl. Phys. Lett. 70 (1997) 280.

[10] F. Firszt, S. Lęgowski, H. Męczyńska, J. Szatkowski, W. Paszkowicz, K. Godwod, J. Cryst. Growth 184/185 (1998) 35.

[11] W. Jackson, N. M. Amer, J. Appl. Phys. 51 (1980) 3343.

[12] M. Maliński, Archives of Acoustics 28 (2003) 43.

[13] J. Zakrzewski, F. Firszt, S. Łęgowski, H. Męczyńska, M. Pawlak, A. Marasek, Rev. Sci. Instrum. 74 (2003) 566.
[14] J. Zakrzewski, M. Malinski, K. Strzałkowski, F. Firszt, S. Łęgowski, H. Męczyńska, A. Marasek, M. Pawlak, J. Phys. IV 137 (2006) 381.
[15] M. Maliński, J. Zakrzewski, K. Strzałkowski, Int. J. Thermophys. 28 (2007) 299.
[16] M. Maliński, J. Zakrzewski, Eur.Phys. J.-Spec. Top. 154 (2008) 345.
[17] J. Zakrzewski, M. Maliński, K. Strzałkowski, F. Firszt, S. Łęgowski, H. Męczyńska, Eur.Phys. J.-Spec. Top. 154 (2008) 381.
[18] J. Zakrzewski, M Maliński, K. Strzałkowski, F. Firszt, S. Łęgowski, H. Męczyńska, A. Marasek, Eur.Phys. J.-Spec. Top. 153 (2008) 267.
[19] M. Malinski, J. Zakrzewski, K. Strzałkowski, S. Łęgowski, F. Firszt, H. Męczyńska, Surf. Sci. 603 (2009) 131.
[20] Ł. Chrobak, M. Maliński, J. Zakrzewski, K. Strzałkowski, Surf. Sci. 603 (2009) 3282.
[21] J. Zakrzewski, M. Malinski, K. Strzałkowski, F. Firszt, S. Łęgowski, H. Męczyńska, Int. J. Thermophys. 31 (2010) 208.
[22] J. Zakrzewski, M. Maliński, K. Strzałkowski, D. Madaj, F. Firszt, S. Łęgowski, H. Męczyńska, Int. J. Thermophys. 33 (2012) 733.
[23] J. Bodzenta, F. Firszt, A. Kaźmierczak-Bałata, M. Pyka, P. Szperlich, M. Szydłowski, J. Zakrzewski, Eur.Phys. J.-Spec. Top. 153 (2008) 139.
[24] M. Pawlak, F. Firszt, S. Łęgowski, H. Męczyńska, J. Gibkes, J. Pelzl, Int. J. Thermophys. 31 (2010) 187.